

On droplet falling velocity

Wenjie Ji¹, Siyuan Wang², Jiguang Hao^{1*}, and J. M. Floryan³

¹School of Aerospace Engineering, Beijing Institute of Technology, Beijing 100081, China

²China Academy of Launch Vehicle Technology, Beijing 100076, China

³Department of Mechanical and Materials Engineering, Western University, London, Ontario N6A 5B9, Canada

Droplet velocities used in impact studies were investigated using high-speed photography. It was determined that droplets do not reach terminal velocity before a typical impact, raising the question of how to predict impact velocity. This question was investigated experimentally, and the results were used to validate a theoretical model. Experiments used droplets with diameters 0.70mm to 4.0mm, liquids with a density of 791kg/m³ to 1261.5kg/m³, and viscosities 1.0mPa s to 1390.0mPa s, release height up to 1.0m. The ambient pressure was varied between atmospheric and 25kPa. It was shown that the droplet velocity increased with the droplet diameter, liquid density, release height, and ambient pressure reduction but changed marginally with viscosity. A simple dynamic model accounting for the aerodynamic drag was proposed. This model, which uses empirical formulae to determine the instantaneous drag coefficient, predicts velocity, which agrees well with the experimental data within the range of parameters used in this study. It provides a valuable tool for the design of droplet impact studies.

1. Introduction

Droplets are widely encountered both in nature and in a variety of applications. Examples include rain¹⁻³, printing⁴⁻⁶, combustion⁷⁻¹⁰, cooling^{11, 12}, coating^{13, 14}, aerosol formation¹⁵, virus spreading¹⁶⁻¹⁹, pesticide delivery¹¹, extraction²⁰ and additive manufacturing²¹⁻²³. Generally, a droplet impacts its target at a specific speed which determines the impact outcomes, i.e., splashing²⁴⁻²⁶, spreading^{27, 28}, or penetration²⁹⁻³¹. No general theoretical method exists to determine the impact velocity as the droplet accelerates just before the impact. As a result, its determination relies on experiments required in various applications, e.g., experimental studies on droplet impact^{25, 30, 32-34}, virus spreading^{17, 18}, printing^{5, 6}, which limits the ability to predict the outcome of droplet impact, e.g., difficulties in determination of safe social distancing. The droplet terminal velocities are well known, but variations of the velocity during the acceleration process are yet to be investigated in detail. As acceleration is rarely finalized in impacts found in applications, this contribution aims to provide a useful theoretical tool for determining the droplet velocity during different stages of its acceleration.

The droplet's acceleration process results from an interplay of its weight, aerodynamic drag, and inertia. The aerodynamic resistance is given as $F_d = 1/8 \rho_g V^2 C_d \pi D^2$ ³⁵ where C_d is the drag coefficient, ρ_g is the air density, V is the droplet velocity, and D is the droplet diameter. For small droplet velocity, F_d is dominated by friction³⁶. As the velocity increases, the aerodynamic (pressure) resistance increases in a complex manner, leading to difficulties in theoretical prediction of the droplet velocity, especially when the pressure is varied³⁷⁻⁴⁰.

It is simple to establish a model to determine the droplet velocity^{41, 42} using Newton's second law if C_d can be determined accurately⁴³. For a spherical body, approximation $C_d = 0.5$ is generally acceptable for small enough Re 's⁴⁴ with deviations increasing as Re increases⁴⁵. For very low Reynolds number $Re = \rho_g V D / \mu_g < 0.1$, C_d can be determined using Stokes' law^{46, 47}. Here, μ_g is the air viscosity. C_d strongly depended on Re for higher Re due to the asymmetry of the pressure field between the upstream and downstream sides of the droplet, with this dependence usually determined experimentally⁴⁸. Various empirical and semi-empirical formulas have been proposed for a wide range of Re 's^{45, 48-61}. However, it is still unclear which formula best predicts the velocity of an accelerating droplet. Additional complications arise for droplets larger than the capillary length as the shape deformation influences C_d ⁶².

Here, we experimentally determined droplet velocity just before its impact as a function of its release height,

diameter, liquid density and viscosity, and ambient air pressure. A simple model to predict this velocity was proposed utilizing an instantaneous C_d . The model was validated through comparison with experiments. It is shown that using an adequately determined C_d leads to a highly accurate prediction of the droplet velocity, providing a useful theoretical tool for its determination under various conditions of interest in droplet impact applications.

2. Experiment

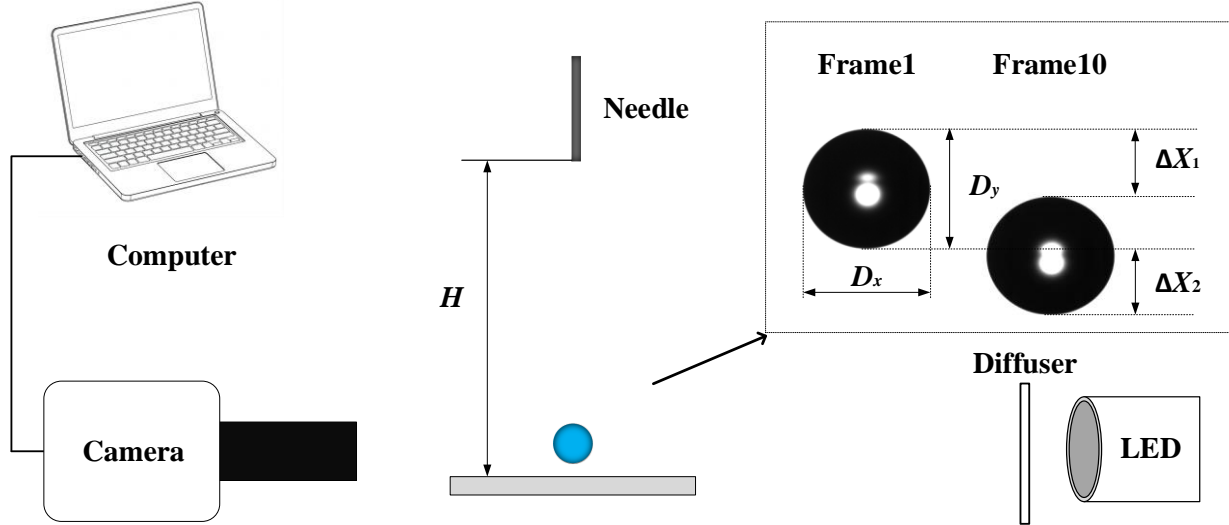


Fig. 1. Sketch of the experimental apparatus. H is the release height. The process used to determine the droplet velocity and diameter is illustrated in the inset. D_x and D_y are the horizontal and vertical droplet diameters, respectively. ΔX_1 and ΔX_2 are the displacements of the upper and lower droplet edges occurring between the tenth and first image frames before the impact, respectively.

As shown in Fig. 1, droplets with diameters ranging from 0.7 to 4.0 mm were generated either using a flat-tipped needle driven by a syringe pump (for $D > 1.8$ mm, dripping method) or using a homemade DOD device³⁰ (for $D < 1.8$ mm). A piezoelectric ceramic buzzer drives the DOD and can produce droplets with diameters ranging from 0.7 to 1.5 mm; see³⁰ for detailed information. Experiments used deionized water, ethanol, and glycerin, with their properties summarized in Table I.

Table I. Physical properties of experimental liquids ($T = 23 \pm 1^\circ\text{C}$)

Liquid	ρ (kg/m ³)	σ (mNm ⁻¹)	μ (mPa s)
Water	998.7	72.9	1.00
Ethanol	791.0	22.9	1.19
Glycerin	1261.5	63.3	1390.00

The release height H was adjusted in a range of 0.1 to 1.0 m for experiments carried out at ambient pressure while in a range of 0.1 to 0.78 m for experiments at reduced pressures. A transparent vacuum chamber controlled the pressure of 10-101 kPa^{25, 39}.

A Photron Nova S12 high-speed camera was used to record the droplet movement and diameter at a rate of 20,000 fps and with a spatial resolution of 12.4 μm /pixel. LEDs combined with a diffuser were used to provide illumination. Experiments were repeated three times for each set of conditions listed in Table II.

Table II. Experimental conditions

set 1: H (m) = 0.1;0.2;0.3;0.4;0.5;0.6;0.8;1.0; set 2: H (m) = 0.1;0.2;0.3;0.4;0.5;0.6;0.78

Number	D (mm)	Liquid	P (kPa)	set
1	0.70	Water	101	1
2	0.93	Water	101	1
3	1.08	Water	101	1
4	1.50	Water	101	1
5	2.30	Water	101	1
6	2.74	Water	101	1
7	3.40	Water	101	1
8	4.00	Water	101	1
9	2.30	Ethanol	101	1
10	2.30	Glycerin	101	1
11	1.84	Ethanol	25/50/75	2
12	2.30	Water	25/50/75	2
13	2.74	Water	25/50/75	2
14	4.00	Water	25/50/75	2

The droplet diameter was calculated^{36, 55, 56} as

$$D = (D_x^2 D_y)^{(1/3)} \quad (1)$$

where D_x and D_y are the horizontal and vertical droplet diameters, respectively; see the inset in Fig. 1. All reported diameter values represent averages from multiple experiments. The droplet velocity was calculated as

$$V = \frac{\Delta X}{\Delta T} \quad (2)$$

where $\Delta X = (\Delta X_1 + \Delta X_2)/2$, ΔX_1 and ΔX_2 are displacements of the upper and lower edges of the droplet between the first and tenth frames 10 the impact (the droplet impacts the plate at frame 11), respectively (see the inset in Fig.1) and $\Delta T = 0.0005$ s is the time for the droplet to move between these frames. The velocities reported here represent averages of three experiments under identical conditions.

3. Theoretical or empirical methods to determine droplet velocity

The acceleration of the droplet is determined by an interplay between its weight, inertia, and aerodynamic resistance. The weight of a spherical droplet is $G = 4/3\pi(D/2)^3\rho g$, where g stands for the gravitational acceleration and ρ is the density of the liquid. The aerodynamic resistance is $F_d = 1/2\pi\rho_g C_d(D/2)^2 V^2$, where ρ_g is the air density. The droplet acceleration is

$$\frac{dV}{dT} = \frac{(G - F_d)}{4/3\pi(D/2)^3\rho} = g - \frac{(3C_d\rho_g V^2)}{4D\rho} \quad (3)$$

where T is time measured from droplet release time, and the droplet velocity can be determined using

$$V = \frac{dH}{dT} \quad (4)$$

In Eq. (3), C_d is the only undetermined parameter. Ignoring resistance results in $C_d = 0$ and $V = \sqrt{2gH}$ which provide limiting values for very low ambient pressure.

In general, C_d is not negligible and is given by an empirical formula^{45, 48, 55}

$$C_d = \frac{24}{Re}(1 + k(Re)) \quad (5)$$

where $k(Re)$ is a Re -dependent correction factor determined experimentally, typically using wind tunnel experiments with spherical solid models; such experiments do not account for droplet deformation, oscillations, and internal dynamics.

For $Re < 1$, the Stokes law is satisfied⁴⁸, i.e., $k(Re) \approx 0$. As D or/and V increases, the pressure effects contribute to the resistance, and the relation $k(Re)$ is usually determined empirically. Fuchs⁶³ proposed an empirical expression

$$C_d = f_1(Re) = \frac{24}{Re}(1 + 0.158Re^{2/3}). \quad (6)$$

This relation has been used in determining the droplet velocity⁴⁴ in the present study, with variations of C_d illustrated using a solid magenta line in Fig. 2.

Yang⁶⁴ collected historical data for C_d for a smooth sphere and used a multigene genetic programming approach to produce correlation (7). C_d prediction based on this correlation yielded the green dashed line in Fig. 2.

$$\begin{cases} C_d = f_2(Re) = R(Re) + err(Re), \\ R(Re) = \frac{24}{Re} \left(1 + \frac{3/16Re}{1 + (19/240Re)/(1 + 1/122Re)} \right), \\ err(Re) = \frac{8}{1000} \frac{\ln[(1+Re)/21000][\ln((1+Re)/254)]^2}{1 + Re/7000}. \end{cases} \quad (7)$$

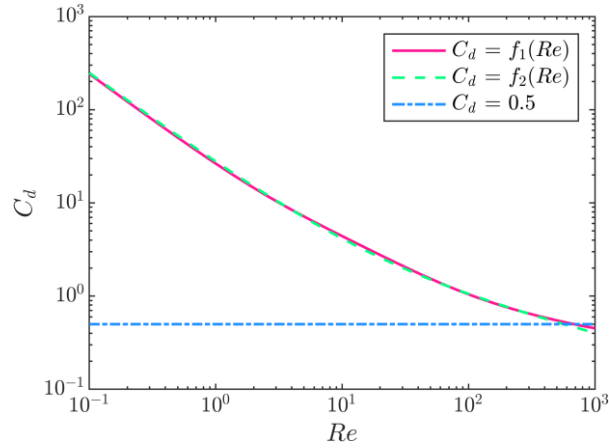


Fig. 2. Variations of the drag coefficient C_d determined using Eq. (6) (the solid magenta line) and (7) (the green dashed line) as a function of Re . The blue dash-dotted line provides the reference value $C_d=0.5$.

A SCILAB code was developed to solve numerically Eqs (3) and (4) for C_d either varying with velocity as described by Eq. (6) or (7) or taken as $C_d = 0.5$. This code evaluated instantaneous C_d and produced V as a function of H with $V = 0.0$, $H = 0.0$, and $T = 0.0$ as initial conditions, 0.001s as the time step, and a specific value of H as the end condition.

Previous studies on droplet impacts used an alternative empirical expression (8)⁶⁵⁻⁶⁹ to determine the droplet velocity for a specific value of H based on its terminal velocity

$$V = V_T \left[1 - \exp\left(\frac{-2gH}{V_T^2}\right) \right]^{\frac{1}{2}} \quad (8)$$

where V_T is a function of droplet diameter and can be determined using the empirical expression^{66, 70} :

$$V_T = 9.65 - 10.3 \exp(-600D) \quad (9)$$

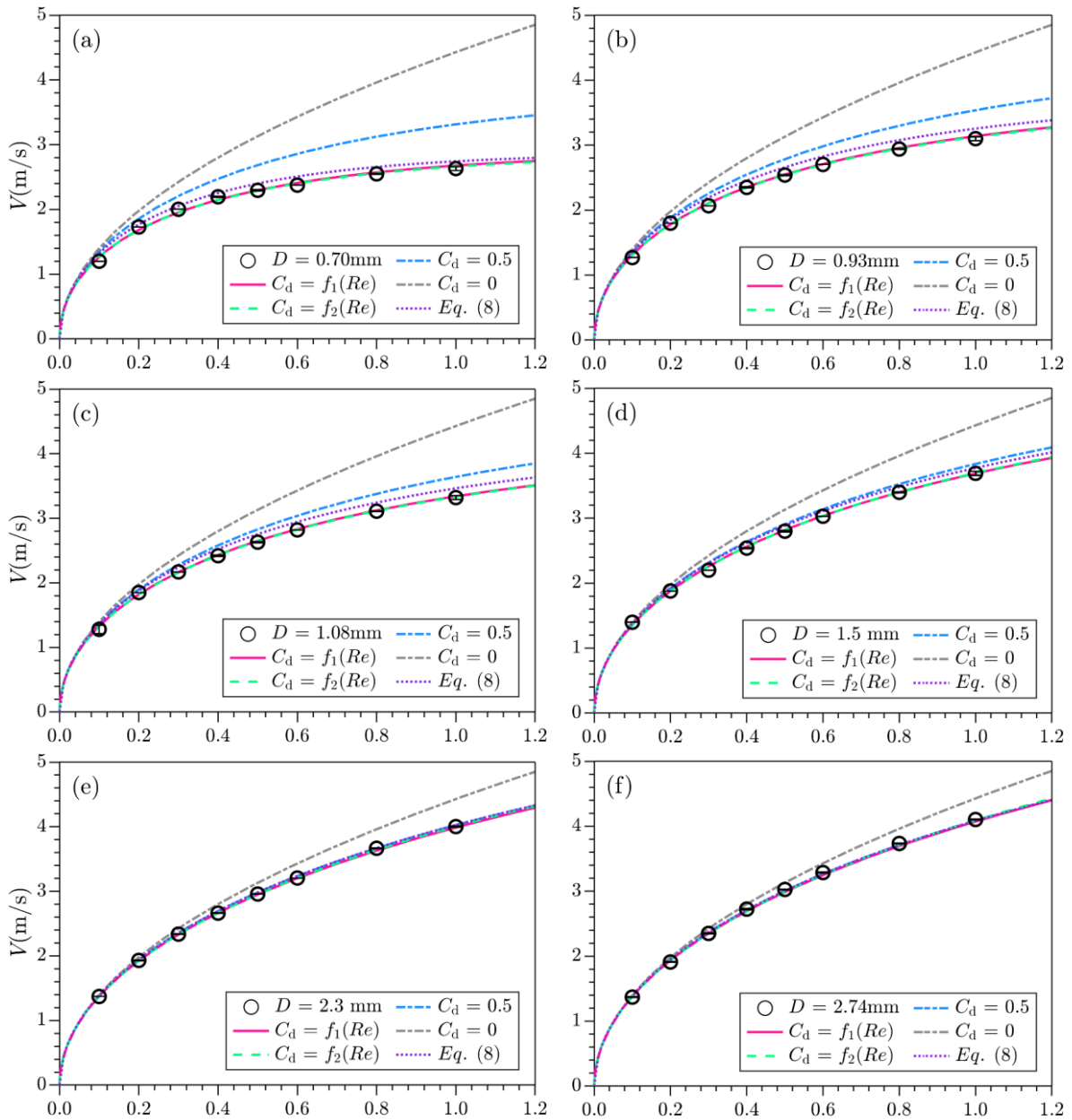
Predictions based on the five models, i.e., $C_d = f_1(Re), f_2(Re), 0, 0.5$, and a combination of Eqs (8) and (9) were

compared with the experimental results to determine the most accurate model.

4. Results

4.1 At ambient pressure

Figure 3 illustrates variations of velocity V of water droplets with diameters of (a) $D = 0.70\text{mm}$, (b) $D = 0.93\text{mm}$, (c) $D = 1.08\text{mm}$, (d) $D = 1.5\text{mm}$, (e) $D = 2.3\text{mm}$, (f) $D = 2.74\text{mm}$, (g) $D = 3.4\text{mm}$, (h) $D = 4.0\text{mm}$ as a function of the release height H at ambient pressure. The velocity increases as an increase of H for all droplet diameters. The bigger the droplet, the larger velocity for the same H . This trend is increasingly evident with the increase of H , indicating that acceleration decreases faster for smaller droplets with an increase of H or V .



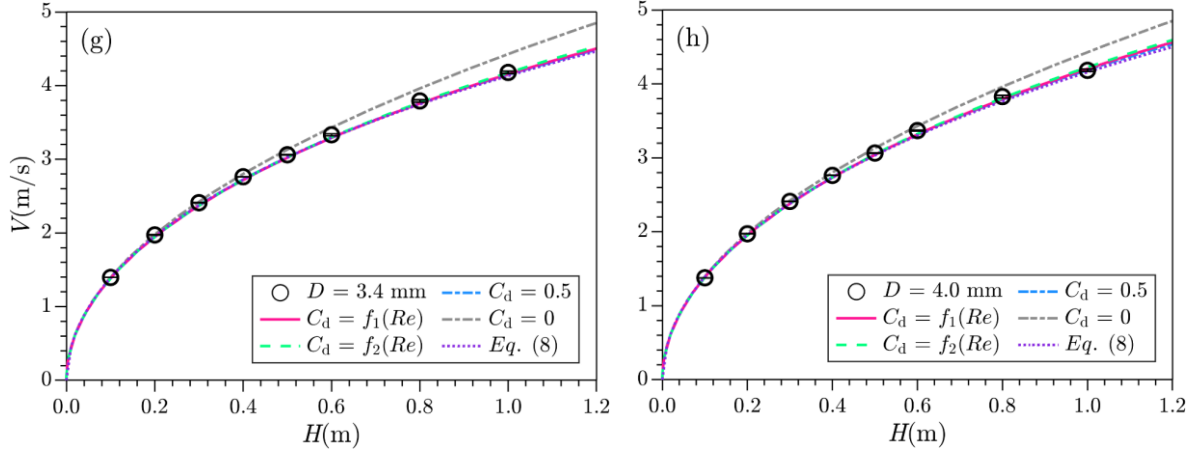


Fig. 3. Variations of V as a function of H for water droplets with diameters (a) $D = 0.70\text{mm}$, (b) $D = 0.93\text{mm}$, (c) $D = 1.08\text{mm}$, (d) $D = 1.50\text{mm}$, (e) $D = 2.30\text{mm}$, (f) $D = 2.74\text{mm}$, (g) $D = 3.40\text{mm}$, (h) $D = 4.00\text{mm}$. Circles identify the experimental points. Error bars indicate the standard deviations. Magenta solid, green dashed, blue, and grey dash-dotted lines represent theoretically determined velocity with C_d determined using Eqs (6) and (7), $C_d=0.5$, and $C_d=0$, respectively. The purple dotted line represents velocity determined using Eqs (8) and (9).

Lines in Fig.3 show the theoretically-determined falling velocities as a function of H using the five models discussed above. The magenta solid and green dashed lines illustrate velocities determined by numerically solving Eqs (3) and (4) using instantaneous C_d determined from Eqs (6) and (7), respectively. They both agree well with the experimental results regardless of the diameters. The grey dash-dotted line illustrates velocity predicted using $C_d = 0$, i.e., with negligible air resistance. Comparison with experimental results shows that the air resistance-induced reduction of the falling velocity is more significant for the smaller droplets and the higher the release height. The blue dash-dotted line illustrates velocity determined using $C_d = 0.5$. The predictions for larger droplets, i.e., $D = 2.3\text{mm}$, 2.74mm , 3.4mm , and 4.0mm , are similar to those obtained using Eqs (6) and (7). The deviation between predictions based on $C_d = 0.5$ and the experimental results increases with a reduction of the droplet diameter, indicating that $C_d=0.5$ produces good results only for a limited range of droplet diameter, i.e., $2.3\text{mm} < D < 4.0\text{mm}$. The purple dotted line illustrates velocities predicted using Eqs (8) and (9) – these predictions fall between those obtained using $C_d = 0$ and 0.5 but are less accurate than those determined using instantaneous C_d 's described by Eqs. (6) and (7), especially for the four smaller droplets. Results produced by all five methods agree well with the experiments for the lowest release height of $H = 0.1\text{m}$ (i.e., smallest droplet velocities), indicating that the air resistance can be neglected for small H with $V = \sqrt{2gH}$ providing a reasonably accurate velocity prediction³⁶. For larger droplets of $D = 3.4\text{mm}$, and 4.0mm , the velocities determined by $V = \sqrt{2gH}$ also agree reasonably with the experiments even for $H = 0.6\text{m}$, indicating that use $V = \sqrt{2gH}$ for velocity predictions is reasonable for large droplet released from $H < 0.6\text{m}$ ⁴⁴.

Figure 4 illustrates variations of velocity V for water droplets as a function of the droplet diameter D for the release height H of 0.8m (a) and 1.0m (b), respectively. It provides intuitive support to the statement above that V increases as an increase of D for the same H , especially for smaller droplets of $D < 2.3\text{mm}$. Predictions based on C_d determined by Eqs (6) and (7) provide the best matching with experimental measurements for all droplet diameters used in this study; predictions based on Eqs (8) and (9) agree with the experiments reasonably. The model using $C_d = 0.5$ produces good results for a droplet diameter range of $2.3\text{mm} < D < 4.0\text{mm}$ with error increasing with a decrease of D . For higher H 's of 0.8m and 1.0m , the method using $C_d = 0$ cannot produce reasonable predictions, especially for small droplets.

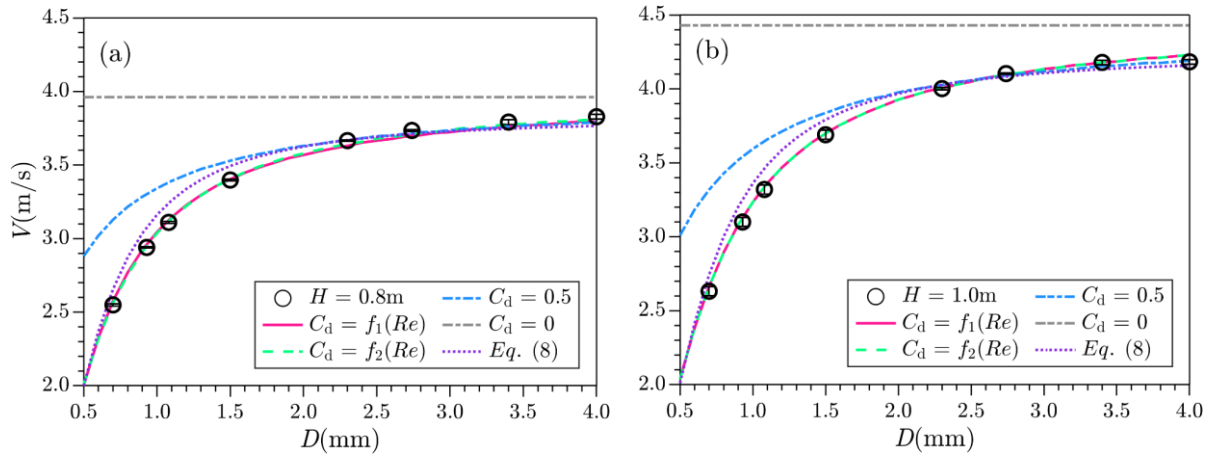


Fig. 4. Variations of velocity V as a function of D for H (a) 0.8 m and (b) 1.0 m. Symbols and lines are the same as in Fig. 3.

Figure 5 illustrates variations of V for ethanol (a) and glycerin (b) droplets of $D = 2.30$ mm as a function of the release height H . Variations of V determined experimentally for ethanol and glycerin exhibit the same trend as the water droplets. Theoretical predictions based on the numerical solution of Eqs (3) and (4) with different instantaneous C_d 's, i.e., 0.5, determined either by Eq. (6) or by Eq. (7), account for droplet density and, thus, produce accurate predictions for droplets made of different liquids. Use of Eqs (8) and (9) produces the same velocities regardless liquid's density; they are larger than those observed experimentally for ethanol but smaller for glycerin droplets.

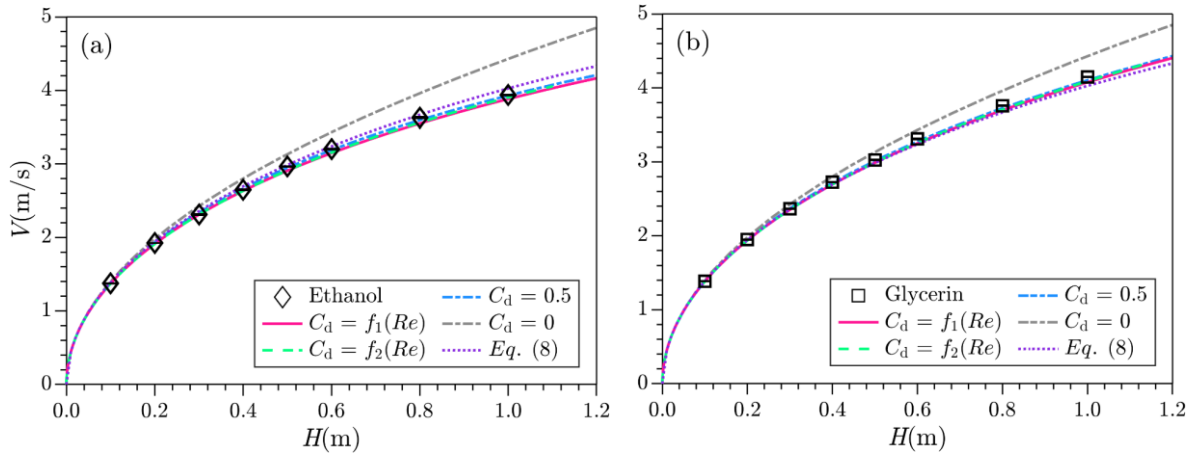


Fig. 5. Variations of velocity V as a function of the release height H for (a) ethanol and (b) glycerin droplets of $D = 2.30$ mm. Diamonds identify experimental points for ethanol, and squares identify experimental points for glycerin. Error bars indicate the standard deviations. The lines are the same as in Fig. 3.

Figure 6 illustrates variations of V for (a) $H = 0.8$ m and (b) 1.0 m as a function of liquid density ρ for droplets with $D = 2.30$ mm. Diamonds (ethanol), circles (water), and squares (glycerin) identify experimental points. Lines illustrate theoretical predictions. Results demonstrate that V increases as an increase of ρ for the same H due to a larger weight increase than the air resistance F_d . Theoretical predictions based on the first three models agree well with this trend, but predictions based on Eqs (8) and (9) are insensitive to density variations, further indicating the limitations of these models.

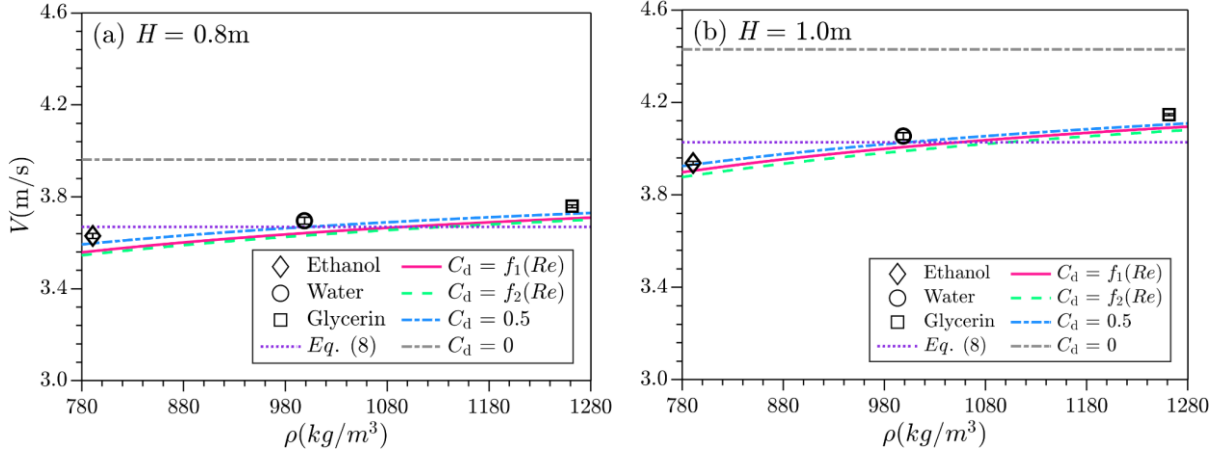


Fig. 6. Variations of velocity V as a function of the droplet density ρ for H (a) 0.8m and (b) 1.0m for $D = 2.30$ mm. Ethanol, water, and glycerin results are identified using diamonds, circles, and squares. Error bars indicate the standard deviations. The lines are the same as in Fig. 3.

4.2 At reduced pressure

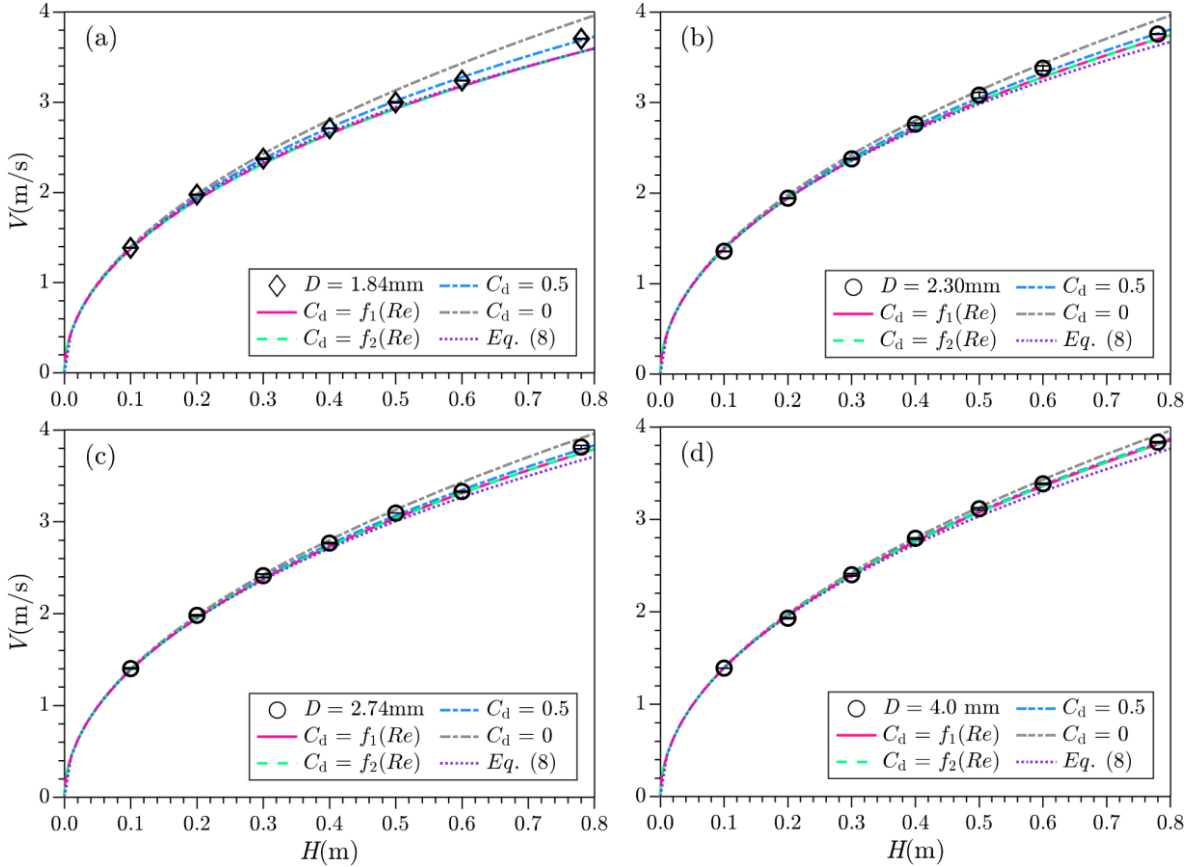


Fig. 7. Variations of velocity V as a function of H for droplets of (a) ethanol with $D = 1.84$ mm, water with (b) $D = 2.3$ mm, (c) $D = 2.74$ mm, (d) $D = 4.0$ mm at $P = 50$ kPa. Diamonds and circles identify the experimental points of ethanol and water. Error bars indicate the standard deviations. Lines are as stated in the caption of Fig. 3.

Figure 7 illustrates variations of velocity V of droplets of (a) ethanol with $D = 1.84$ mm, water with (b) $D = 2.30$ mm, (c) $D = 2.74$ mm, and (d) $D = 4.00$ mm as functions H at a reduced pressure of $P = 50$ kPa. It was not possible to experiment with smaller droplets since the DOD cannot work at reduced pressure due to the formation

of air bubbles from dissolved air. Compared with the results at ambient pressure, the results are closer to predictions based on $C_d = 0$ (the grey dash-dotted line), indicating that the reduced pressure decreases the air resistance. To consider the air pressure, the first three models determine the air density using the ideal-gas state equation and produce predictions that agree well with the experiments. Predictions based on Eqs (8) and (9) remain unchanged as these relations cannot account for air pressure variations.

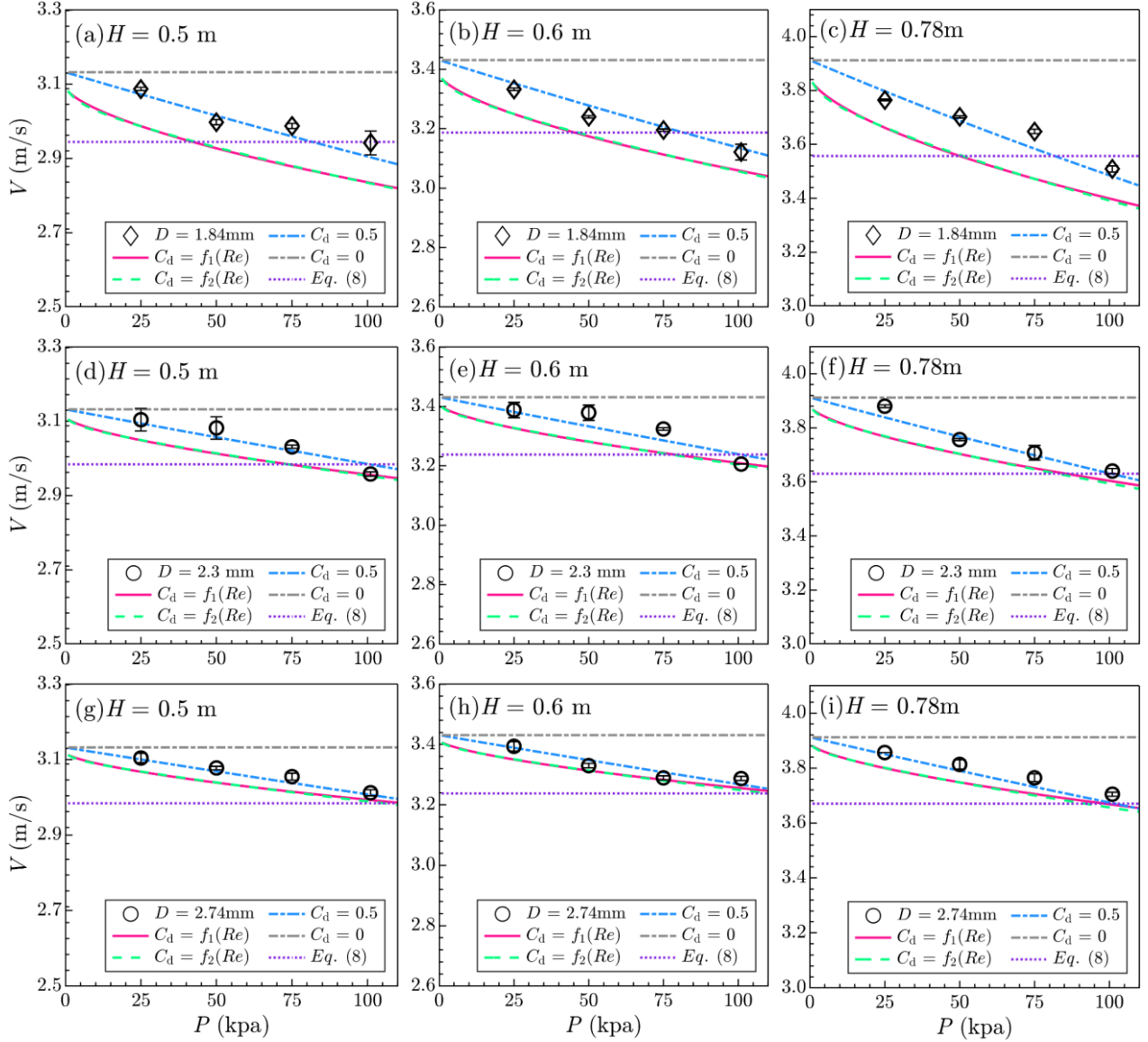


Fig. 8. Variations of velocity V as a function of the air pressure P for ethanol droplets with $D = 1.84\text{mm}$ for $H = 0.5\text{m}$ (a), 0.6m (b), and 0.78m (c), for water droplets with $D = 2.3\text{mm}$ for $H = 0.5\text{m}$ (d), 0.6m (e) and 0.78m (f), and for water droplets with $D = 2.74\text{mm}$ for $H = 0.5\text{m}$ (g), 0.6m (h) and 0.78m (i). Diamonds and circles identify the experimental points for ethanol and water. Error bars indicate the standard deviations. Lines are as stated in the caption of Fig. 3.

Figure 8 illustrates variations of velocity V for ethanol droplets with $D = 1.84\text{ mm}$ released at (a) $H = 0.5\text{m}$, (b) $H = 0.6\text{m}$, and (c) $H = 0.78\text{m}$ (c) for water droplets with $D = 2.3\text{ mm}$ released at (d) $H = 0.5\text{m}$, (e) $H = 0.6\text{m}$, and (f) $H = 0.78\text{m}$, for water droplets with $D = 2.74\text{ mm}$ released at (g) $H = 0.5\text{m}$, (h) $H = 0.6\text{m}$, and (i) $H = 0.78\text{m}$ as functions of the air pressure P . V increases nearly linearly with a decrease of P for various H 's and D 's; this increase is larger for larger H 's and smaller D 's, indicating a stronger air resistance for the two situations. The reader

may note that V increases from 2.94 m/s to 3.09 m/s for ethanol droplets with $D = 1.84\text{mm}$ released from $H = 0.5\text{m}$ (Fig. 8 (a)), but from 3.51 m/s to 3.76 m/s for droplets released from $H = 0.78\text{m}$ (Fig. 8 (c)); V increases from 2.96 m/s to 3.10 m/s for water droplets with $D = 2.30\text{mm}$ released from $H = 0.5\text{m}$ (Fig. 8 (d)), but from 3.01 m/s to 3.10 m/s for droplets with $D = 2.74\text{mm}$ (Fig. 8 (g)).

Predictions using $C_d = 0$ and Eqs (8) and (9) are unaffected by air pressure, indicating that they cannot account for pressure variations. Predictions based on Eqs (6) and (7) start from $P = 1\text{ kPa}$ in Fig.8 as the continuum model fails for rarified gases ($P \rightarrow 0$). The predictions produced by the first three models agree reasonably with the experiments, indicating their wide adaptability.

5. Conclusion

The velocity of the falling droplet just before its impact was determined experimentally for a range of droplet diameters, liquid density, release height and air pressure. The existing correlations for predicting droplet velocity were compared with the experimental results. It is shown that predictions produced by a dynamic model that utilizes the instantaneous values of the drag coefficient from two empirical correlations agree well with all the experiments in the range of parameters used in this study, providing a valuable tool for the determination of the droplet velocity used in impact studies.

Acknowledgments

This study was financially supported by the National Natural Science Foundation of China under Grant No. 12072032, the National Key R&D Program of China under Grant No. 2018YFF0300804, and 111 Project under Grant No. B16003.

*hjgizq@bit.edu.cn

References

1. D. Soto, A. B. De Larivière, X. Boutillon, C. Clanet, and D. Quéré, "The force of impacting rain," *Soft Matter*. **10**, 4929 (2014).
2. X. Cheng, T.-P. Sun, and L. Gordillo, "Drop impact dynamics: impact force and stress distributions," *Annu. Rev. Fluid Mech.* **54**, 57 (2022).
3. S. T. Thoroddsen, T. G. Etoh, and K. Takehara, "High-speed imaging of drops and bubbles," *Annu. Rev. Fluid Mech.* **40**, 257 (2008).
4. H. Abdolmaleki, P. Kidmose, and S. Agarwala, "Droplet-Based Techniques for Printing of Functional Inks for Flexible Physical Sensors," *Adv Mater.* **33**, 2006792 (2021).
5. D. B. van Dam, and C. L. Clerc, "Experimental study of the impact of an ink-jet printed droplet on a solid substrate," *Phys. Fluids*. **16**, 3403 (2004).
6. D. Lohse, "Fundamental fluid dynamics challenges in inkjet printing," *Annu. Rev. Fluid Mech.* **54**, 349 (2022).
7. A. Williams, "Combustion of droplets of liquid fuels: a review," *Combust. Flame*. **21**, 1 (1973).
8. C. Josserand, and S. T. Thoroddsen, "Drop impact on a solid surface," *Annu. Rev. Fluid Mech.* **48**, 365 (2016).
9. D. Quéré, "Leidenfrost dynamics," *Annu. Rev. Fluid Mech.* **45**, 197 (2013).
10. G. Liang, and I. Mudawar, "Review of drop impact on heated walls," *Int. J. Heat Mass Transfer*. **106**, 103 (2017).
11. A. L. Yarin, "Drop impact dynamics: splashing, spreading, receding, bouncing...", *Annu. Rev. Fluid Mech.* **38**, 159 (2006).
12. W. Jia, and H. H. Qiu, "Experimental investigation of droplet dynamics and heat transfer in spray cooling," *Exp. Therm Fluid Sci.* **27**, 829 (2003).
13. S. Ren, S. Wang, Z. Dong, J. Chen, and L. Li, "Dynamic behaviors and self-cleaning property of droplet on superhydrophobic coating in uniform DC electric field," *Colloids Surf. A Physicochem. Eng. Aspect.* **626**, 127056

(2021).

14. J. Chen, J. Chen, L. Li, S. Wang, and Y. Xie, "Droplet rolling angle model of micro-nanostructure superhydrophobic coating surface," *Eur. Phys. J. E.* **44**, 25 (2021).
15. P. Mirbod, E. A. Haffner, M. Bagheri, and J. E. Higham, "Aerosol formation due to a dental procedure: insights leading to the transmission of diseases to the environment," *J R Soc Interface.* **18**, 20200967 (2021).
16. L. Xu, S. Zong, J. Hao, and J. Floryan, "Droplet penetration through an inclined mesh," *Phys. Fluids.* **12**, 122105 (2022).
17. R. Mittal, R. Ni, and J.-H. Seo, "The flow physics of COVID-19," *J. Fluid Mech.* **894**, F2 (2020).
18. L. Bourouiba, "The fluid dynamics of disease transmission," *Annu. Rev. Fluid Mech.* **53**, 473 (2021).
19. M. Zhou, and J. Zou, "A dynamical overview of droplets in the transmission of respiratory infectious diseases," *Phys. Fluids.* **33**, 031301 (2021).
20. P. Mary, V. Studer, and P. Tabeling, "Microfluidic droplet-based liquid–liquid extraction," *Anal. Chem.* **80**, 2680 (2008).
21. L. E. Murr, and W. L. Johnson, "3D metal droplet printing development and advanced materials additive manufacturing," *J. Mater. Res. Technol.* **6**, 77 (2017).
22. S. Fathi, P. Dickens, and F. Fouchal, "Regimes of droplet train impact on a moving surface in an additive manufacturing process," *J. Mater. Process. Technol.* **210**, 550 (2010).
23. T. Colton, and N. B. Crane, "Influence of droplet velocity, spacing, and inter-arrival time on line formation and saturation in binder jet additive manufacturing," *Addit. Manuf.* **37**, 101711 (2021).
24. L. Xu, W. W. Zhang, and S. R. Nagel, "Drop splashing on a dry smooth surface," *Phys. Rev. Lett.* **94**, 184505 (2005).
25. J. Hao, J. Lu, L. Lee, Z. Wu, G. Hu, and J. M. Floryan, "Droplet splashing on an inclined surface," *Phys. Rev. Lett.* **122**, 054501 (2019).
26. G. Riboux, and J. M. Gordillo, "The diameters and velocities of the droplets ejected after splashing," *J. Fluid Mech.* **772**, 630 (2015).
27. Y. Cheng, E. Li, J. Wang, P. Yu, and Y. Sui, "Rapid droplet spreading on a hot substrate," *Phys. Fluids.* **33**, 092103 (2021).
28. Y. Song, Q. Wang, Y. Ying, Z. You, S. Wang, J. Chun, X. Ma, and R. Wen, "Droplet spreading characteristics on ultra-slippery solid hydrophilic surfaces with ultra-low contact angle hysteresis," *Coatings.* **12**, 755 (2022).
29. L. Xu, W. Ji, J. Lu, Y. Li, J. Hao, G. Hu, and J. M. Floryan, "Droplet impact on a prewetted mesh," *Phys. Rev. Fluids.* **6**, L101602 (2021).
30. A. Abouei Mehrizi, S. Lin, L. Sun, and L. Chen, "Spectacular behavior of a viscoelastic droplet impinging on a superhydrophobic mesh," *Langmuir.* **38**, 6106 (2022).
31. G. Vadlamudi, S. Thirumalaikumaran, D. Chakravorty, A. Saha, and S. Basu, "Penetration and aerosolization of cough droplet spray through face masks: A unique pathway of transmission of infection," *Phys. Fluids.* **34**, 052108 (2022).
32. R. Payri, B. Tormos, F. J. Salvador, and L. Araneo, "Spray droplet velocity characterization for convergent nozzles with three different diameters," *Fuel.* **87**, 3176 (2008).
33. A. R. Esmaili, G. Meisoll, N. Mir, and R. Mohammadi, "On the droplet impact dynamics of nonionic surfactant solutions on non-wettable coatings," *J. Colloid Interface Sci.* **623**, 1039 (2022).
34. B. Gorin, D. Bonn, and H. Kellay, "Droplet impacts on cold surfaces," *J. Fluid Mech.* **944**, A23 (2022).
35. R. Clift, and W. H. Gauvin, "Motion of entrained particles in gas streams," *Can J Chem Eng.* **49**, 439 (1971).
36. Z. Wu, J. Hao, J. Lu, L. Xu, G. Hu, and J. M. Floryan, "Small droplet bouncing on a deep pool," *Phys. Fluids.* **32**, 012107 (2020).
37. Y. Cao, and M. Xin, "Numerical simulation of supercooled large droplet icing phenomenon: a review," *Arch.*

Comput. Methods Eng. **27**, 1231 (2019).

38. S. Zhou, and L. Zhang, "Research on airflow optimization and infection risk assessment of medical cabin of negative-pressure ambulance," *Sustainability*. **14**, 4900 (2022).

39. J. Hao, J. Lu, Z. Zhang, Z. Wu, G. Hu, and J. M. Floryan, "Asymmetric droplet splashing," *Phys. Rev. Fluids*. **5**, 073603 (2020).

40. L. Xu, L. Barcos, and S. R. Nagel, "Splashing of liquids: Interplay of surface roughness with surrounding gas," *Phys. Rev. E*. **76**, 066311 (2007).

41. G. D. Kinzer, and R. Gunn, "The evaporation, temperature and thermal relaxation-time of freely falling waterdrops," *J. Meteorol.* **8**, 71 (1951).

42. G. Lorenzini, "Simplified modelling of sprinkler droplet dynamics," *Biosyst. Eng.* **87**, 1 (2004).

43. K. Hayashi, and A. Tomiyama, "A drag correlation of fluid particles rising through stagnant liquids in vertical pipes at intermediate reynolds numbers," *hem. Eng. Sci.* **64**, 3019 (2009).

44. K. Range, and F. Feuillebois, "Influence of surface roughness on liquid drop impact," *J. Colloid Interface Sci.* **203**, 16 (1998).

45. K. Ceylan, A. Altunbaş, and G. Kelbaliyev, "A new model for estimation of drag force in the flow of Newtonian fluids around rigid or deformable particles," *Powder Technol.* **119**, 250 (2001).

46. W. W. Rubey, "Settling velocity of gravel, sand, and silt particles," *Am. J. Sci.* **5**, 325 (1933).

47. F. Engelund, and E. Hansen, *A monograph on sediment transport in alluvial streams* (Danish Technical Press, Copenhagen, 1967).

48. G. Kelbaliyev, and K. Ceylan, "Development of new empirical equations for estimation of drag coefficient, shape deformation, and rising velocity of gas bubbles or liquid drops," *Chem. Eng. Commun.* **194**, 1623 (2007).

49. J. L. Buzzard, and R. M. Nedderman, "The drag coefficients of liquid droplets accelerating through air," *Chem. Eng. Sci.* **22**, 1577 (1967).

50. B. G. Cox, "On driving a viscous fluid out of a tube," *J. Fluid Mech.* **14**, 81 (2006).

51. R. M. Wellek, A. K. Agrawal, and A. H. P. Skelland, "Shape of liquid drops moving in liquid media," *AIChE J.* **12**, 854 (1966).

52. J. R. Garratt, "Review of drag coefficients over oceans and continents," *Mon. Weather Rev.* **105**, 915 (1977).

53. M. Aminzadeh, A. Maleki, B. Firoozabadi, and H. Afshin, "On the motion of newtonian and non-newtonian liquid drops," *Sci. Iran.* **19**, 1265 (2012).

54. Z.-G. Feng, and E. E. Michaelides, "Drag coefficients of viscous spheres at intermediate and high reynolds numbers," *J. Fluids Eng.* **123**, 841 (2001).

55. J. A. Mulholland, R. K. Srivastava, and J. O. L. Wendt, "Influence of droplet spacing on drag coefficient in nonevaporating, monodisperse streams," *AIAA J.* **26**, 1231 (1988).

56. J. R. G. R. Clift, and M. E. Weber, *Bubbles, drops, and particles* (Academic Press, New York, 1978).

57. S. A. Morsi, and A. J. Alexander, "An investigation of particle trajectories in two-phase flow systems," *J. Fluid Mech.* **55**, 193 (2006).

58. R. Turton, and O. Levenspiel, "A short note on the drag correlation for spheres," *Powder Technol.* **47**, 83 (1986).

59. P. K. Swamee, and C. S. P. Ojha, "Drag coefficient and fall velocity of nonspherical particles," *J. Hydraul. Eng.* **117**, 660 (1991).

60. A. R. Khan, and J. F. Richardson, "The resistance to motion of a solid sphere in a fluid," *Chem. Eng. Commun.* **62**, 135 (2007).

61. W. R. A. Goossens, "Review of the empirical correlations for the drag coefficient of rigid spheres," *Powder Technol.* **352**, 350 (2019).

62. Y. Lin, and J. Palmore, "Effect of droplet deformation and internal circulation on drag coefficient," *Phys. Rev. Fluids.* **7**, (2022).

63. N. A. Fuchs, R. Daisley, M. Fuchs, C. Davies, and M. Straumanis, "The mechanics of aerosols," *Phys. Today*. **18**, 73 (1965).
64. H. Yang, M. Fan, A. Liu, and L. Dong, "General formulas for drag coefficient and settling velocity of sphere based on theoretical law," *Int. J. Min. Sci. Technol.* **25**, 219 (2015).
65. T. Kurniawan, P.-H. Tsai, S.-S. Chen, D. H. Frakes, C.-C. Chen, and A.-B. Wang, "Practical notes toward higher quality and more reliable experiments on drop and liquid surface interactions," *Exp. Fluids*. **63**, 8 (2022).
66. J. Saylor, and N. Grizzard, "The optimal drop shape for vortices generated by drop impacts: the effect of surfactants on the drop surface," *Exp. Fluids*. **36**, 783 (2004).
67. H. C. Pumphrey, and P. A. Elmore, "The entrainment of bubbles by drop impacts," *J. Fluid Mech.* **220**, 539 (1990).
68. H. C. Pumphrey, L. A. Crum, and L. Bjornhoj, "Underwater sound produced by individual drop impacts and rainfall," *J Acoust Soc Am.* **85**, 1518 (1989).
69. M. J. Thoraval, K. Takehara, T. G. Etoh, and S. T. Thoroddsen, "Drop impact entrapment of bubble rings," *J. Fluid Mech.* **724**, 234 (2013).
70. D. Atlas, R. Srivastava, and R. S. Sekhon, "Doppler radar characteristics of precipitation at vertical incidence," *Rev. Geophys.* **11**, 1 (1973).